

THE TRANSVERSE VELOCITY STRUCTURE OF THE HH 111 JET¹

A. Riera,^{2,3} R. López,³ A. C. Raga,⁴ G. Anglada,⁵ and R. Estalella³

Received 2001 February 6; accepted 2001 April 5

RESUMEN

Presentamos espectroscopía de rendija larga del jet HH 111, obtenida con el telescopio William Herschel, de 4.2 m de diámetro. Hemos obtenido espectros con posiciones de la rendija a lo largo y a través del jet, con la finalidad de buscar variaciones de la velocidad, densidad electrónica y excitación a través del jet. Hemos detectado emisión débil en los nudos HH 111 D y F, extendiéndose a grandes distancias ($\approx 15''$) del eje de flujo. Esta emisión extendida presenta una estratificación en velocidad, encontrándose las velocidades más altas sobre el eje del jet, y disminuyendo al alejarse de dicho eje. El nudo D tiene una densidad electrónica central baja, rodeado por material de densidad electrónica mayor, mientras que el nudo F tiene una densidad electrónica aproximadamente constante. Argumentamos que la emisión extendida y las variaciones de velocidad observadas con la distancia al eje del jet de HH 111 son compatibles con un jet que presenta un gradiente transversal de velocidad en su haz, o con un jet que está incorporando material de baja velocidad.

ABSTRACT

We present long-slit spectroscopic observations of the HH 111 jet obtained with the 4.2 m William Herschel Telescope. We have obtained spectra for slit positions along and across the jet axis, in order to search for radial velocity, electron density and excitation variations across the jet. We have detected faint emission across knots HH 111 D and F, extending to large ($\approx 15''$) distances from the flow axis. This extended emission shows a radial velocity stratification, with higher radial velocities on the jet axis and lower velocities away from the axis. Knot D has a low central electron density surrounded by material with higher electron densities, while the electron density is approximately constant across knot F. We argue that the extended emission and the radial velocity variations observed across the HH 111 flow are compatible with a jet beam with a transverse gradient in velocity or with a jet which is entraining low velocity material.

Key Words: **ISM: INDIVIDUAL (HH 111) — ISM: JETS AND OUTFLOWS — STARS: PRE-MAIN-SEQUENCE**

1. INTRODUCTION

Several studies of the kinematics of Herbig-Haro (HH) jets have been made in the past. For example, high resolution spectroscopic studies of the HH 34 (Heathcote & Reipurth 1992), HH 46/47 (Meaburn & Dyson 1987) and HH 111 jets (Reipurth et al. 1997) have been carried out, as well as proper motion measurements for the knots along these jets (HH 34: Eislöffel & Mundt 1992, Heathcote & Reipurth 1992; HH 46/47: Eislöffel & Mundt 1994; HH 111: Reipurth, Raga, & Heathcote 1992).

However, the radial velocity measurements have mostly been limited to a single slit position along

¹Based on observations made with the 4.2 m William Herschel Telescope operated on la Palma by the Isaac Newton Group of Telescopes at the Observatorio del Roque de los Muchachos of the Instituto de Astrofísica de Canarias. Partially based on observations made with the NASA/ESA *Hubble Space Telescope*, obtained from the data archive at the Space Telescope Science Institute. STScI is operated by the Association of Universities for Research in Astronomy, Inc., under NASA contract NAS 5-26555.

²Departament de Física i Enginyeria Nuclear, Universitat Politècnica de Catalunya, Spain.

³Departament d'Astronomia i Meteorologia, Universitat de Barcelona, Spain.

⁴Instituto de Astronomía, Universidad Nacional Autónoma de México.

⁵Instituto de Astrofísica de Andalucía, CSIC, Spain.

the outflow axis. A notable exception is the study of HH 46/47 of Hartigan et al. (1993), who present Fabry-Perot observations which show a strong velocity stratification across the beam of the jet. Morse et al. (1993) present Fabry-Perot observations of the HH 111 jet, but limit their discussion to the structure along the jet, and do not discuss the velocity structure across the jet.

The Fabry-Perot observations of the HH 46/47 jet of Hartigan et al. (1993) show a quite dramatic decrease in radial velocity with distance from the jet axis. This velocity structure across the jet has been interpreted as evidence for turbulent entrainment occurring along the sides of the jet beam (Raymond et al. 1994). However, the HH 46/47 jet has a quite complex morphology, and studies of the radial velocity structure across one of the well aligned jets (such as HH 34 or HH 111) have not yet been carried out.

A somewhat similar effect has been seen in the so-called “microjets” which extend for a few arcseconds away from some T Tauri stars. For example, in the DG Tau microjet (HH 158), a variation in velocity in the transverse direction to the flow, with the velocity increasing toward the flow axis, has been detected within $\approx 3''$ from the source (Lavalley, Cabrit, & Dougados 1997; Lavalley-Fouquet, Cabrit, & Dougados 2000; Bacciotti et al. 2000), and also at $\approx 6''$ from the source (Mundt, Brugel, & Bührke 1987). This radial velocity structure has been interpreted as evidence for the presence of a slower, less collimated, wind surrounding the high velocity jet.

In this paper, we present the results obtained from long-slit high resolution spectroscopy of the HH 111 jet. In this study, we have obtained spectra for slit positions both along and across the jet beam, allowing us to measure the radial velocities and line ratios through the cross-section of the jet. The observations are described in § 2, and the results are presented in § 3. Finally, we discuss these results in § 4.

2. OBSERVATIONS

Long-slit, high resolution spectra of the HH 111 jet were obtained during the night of December 12, 1998. The red arm of the double-armed spectrograph ISIS (Carter et al. 1994) and a Tektronics CCD detector of 1024×1024 pixels (pixel size of $24 \mu\text{m}$) were used at the Cassegrain focus of the 4.2 m William Herschel Telescope (WHT) at the Observatorio del Roque de los Muchachos (La Palma, Spain). The high resolution grating R1200R (dispersion 17 \AA mm^{-1}) centered at 6600 \AA was employed, covering the $\text{H}\alpha$, $[\text{N II}] 6548, 6583 \text{ \AA}$ and $[\text{S II}] 6717, 6731 \text{ \AA}$ lines and providing a spectral res-

olution of $0.41 \text{ \AA pixel}^{-1}$ (equivalent to 20 km s^{-1} at $\text{H}\alpha$ for a $1''$ slit width). The spatial resolution was $0.36'' \text{ pixel}^{-1}$ and the seeing had a FWHM of $2''$ to $3''$ during the night. The spectrograph slit had a projected length of $4'$ and a width of $1''.5$, giving an effective spectral resolution of 30 km s^{-1} .

Three spectra were obtained. The first spectrum was obtained with the slit positioned along the central axis of the jet with a P.A. of 97° (slit 1, see Figure 1), with a 1800 s exposure time. The other two slits were placed perpendicular to the jet axis with a P.A. of 7° , cutting the jet beam. A 1800 s exposure was obtained for a slit position cutting the HH 111 jet at the position of knot F (slit 2, see Figure 1), and a 3000 s exposure was obtained for a slit position cutting the jet approximately at the position of knot D (slit 3, see Figure 1).

Individual spectra were corrected for bias, flat-field and cosmic ray events (by median filtering multiple exposures), and were calibrated in wavelength following the standard procedures. The spectra were not flux calibrated. The results obtained from these observations are described in the following section.

3. RESULTS

3.1. Structure along the HH 111 Jet

In Figure 2, we present the $[\text{S II}] 6731 \text{ \AA}$ position-velocity diagram (panel *a*), radial velocities (panel *b*), as well as the $[\text{S II}] 6717/6731$ and $[\text{S II}] (6717+6731)/\text{H}\alpha$ ratios (panels *c* and *d*, respectively) as a function of distance from the position of the VLA source (Rodríguez & Reipurth 1994), which is believed to eject the HH 111 flow. These measurements were obtained with the slit along the jet axis (position 1, see Fig. 1), and are broadly consistent with the results obtained by Morse et al. (1993), who measured position-dependent line ratios, and Reipurth et al. (1997), who present $\text{H}\alpha$ and $[\text{S II}]$ position-velocity diagrams.

In Figure 2*b* we show the velocity of the peak of $[\text{S II}] 6731 \text{ \AA}$ line as a function of the position along the jet axis (solid line), and the velocities at which the line intensity has dropped to half the peak value (dashed lines). We have not attempted to carry out fits with a parametric function since the line profiles are quite asymmetrical. We find that the radial velocity starts with a value of $\approx -20 \text{ km s}^{-1}$ at a distance of $x \approx 15''$ from the source, and becomes more negative until a value of $\approx -70 \text{ km s}^{-1}$ is attained at a distance of $x \approx 24''$ from the source. At larger distances from the source, the radial velocity remains approximately constant, until a sharp drop to a velocity of $\approx -30 \text{ km s}^{-1}$ occurs at the position of knot M ($x \approx 47''$). Beyond knot M, the radial ve-

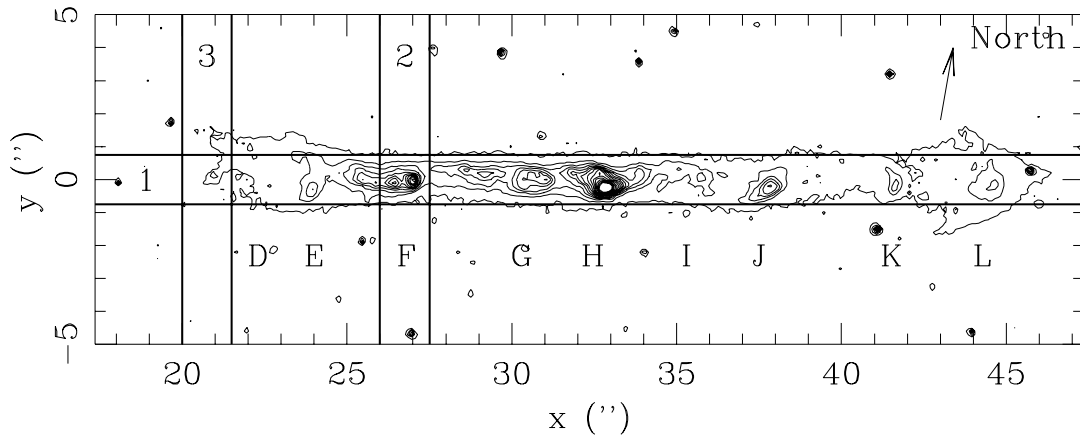


Fig. 1. [S II] 6717+6731 narrow band image from the *HST* archive (see also Reipurth et al. 1997) showing the region within $50''$ from the source of the HH 111 jet (depicted with linear contours). The positions of our three spectrograph slits (labeled 1, 2 and 3, also see the text) are shown. The x and y coordinates are given as offsets (in arcseconds) from the position of the outflow source (see Rodríguez & Reipurth 1994).

locity remains approximately constant, with values ranging from -30 to -40 km s $^{-1}$.

We have also detected redshifted emission from the counterjet at a distance of $48''$ from the central source (see Fig. 2), which corresponds to the position of knot ZL detected in H $_2$ by Gredel & Reipurth (1994). In knot ZL the peak of the [S II] 6731 Å occurs at a heliocentric velocity of 60 km s $^{-1}$.

The width of the [S II] 6731 Å line decreases from a value of ≈ 140 km s $^{-1}$ at $x \approx 15''$ to a value of ≈ 70 km s $^{-1}$ at $x \approx 30''$ (see Fig. 2b). At larger distances from the source, the line width remains approximately constant. The knot ZL has a velocity dispersion of 55 km s $^{-1}$, which is significantly lower than the velocity dispersions measured in the jet. We should note that these line widths are well resolved by our 30 km s $^{-1}$ effective spectral resolution.

Figure 2c shows the density-sensitive [S II] 6717/6731 line ratio. The electron densities are computed from the [S II] 6717/6731 emission line ratios following the standard procedure (Aller 1984). This ratio increases, and consequently the electron density decreases, as a function of increasing distance x from the source, from [S II] 6717/6731 = 0.60 ± 0.10 ($n_e \approx 4500$ cm $^{-3}$) at $x \approx 8''$ to [S II] 6717/6731 = 0.90 ± 0.10 ($n_e \approx 1000$ cm $^{-3}$) in the $13'' < x < 22''$ region. In the $24'' < x < 32''$ region (which covers knots F and H), the line ratio is somewhat lower ([S II] 6717/6731 = 0.75 ± 0.05), corresponding to a $n_e \approx 2000$ cm $^{-3}$. At larger distances from the

source, the measured line ratio grows more or less monotonically, reaching a value of 1.3 (corresponding to $n_e \approx 200$ cm $^{-3}$) in knot P (at $x \approx 74''$). In knot ZL (at $x \approx -48''$ along the counterjet) the measured [S II] line ratio corresponds to $n_e \approx 2000$ cm $^{-3}$. The variation of the electron density with distance to the source is significant within the errors, since for a [S II] 6717/6731 value of ~ 0.75 an uncertainty in the [S II] ratio of 0.05 translates to a 20% uncertainty in the electron density. These results are roughly consistent with the electron densities measured by Reipurth (1989) and Morse et al. (1993).

Figure 2d shows the [S II] (6717+6731)/H α line ratio as a function of distance x from the source. This line ratio has values of ≈ 3 -5 in the brighter knots of the HH 111 jet (knots H, J, K, O, and P) and has lower values of ≈ 2 in the fainter regions (knots D, F, M, and N). Along knot ZL ($-45'' > x > -50''$) the value of the [S II] (6717+6731)/H α line ratio decreases from 4 to 2 with increasing distance from the star.

3.2. Structure across the HH 111 Jet

Figure 3 shows the [S II] 6731 Å position-velocity diagram (panel a), radial velocity (panel b), H α intensity profile (panel c), and different line ratios (panels d and e) obtained from measurements in a slit perpendicular to the jet axis, that intersects the jet at knot F (slit 2, see Fig. 1). Figure 4 shows the same parameters, obtained from measurements across knot D (slit 3 in Fig. 1).

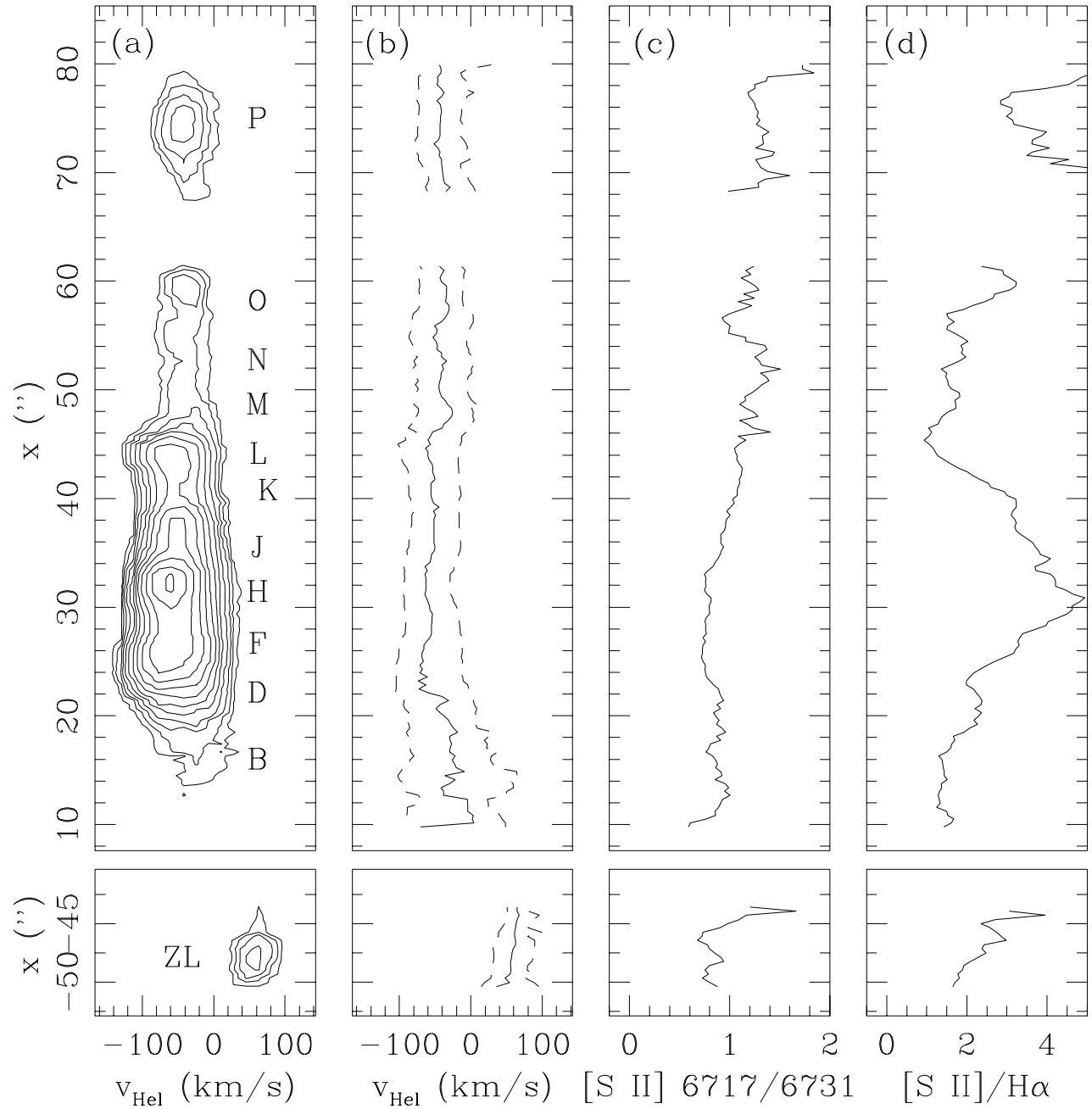


Fig. 2. *a*: [S II] 6731 long slit spectrum along the length of the HH 111 jet (slit position 1 of Figure 1), depicted with factor of $\sqrt{2}$, logarithmic contours. The knots B to P along the blueshifted jet are shown in the upper part of the graph with positive x -values, and the emission along the redshifted counterjet is shown in the lower part of the graph, with negative x -values and a different angular scale. *b*: The heliocentric radial velocity corresponding to the peak of the line profile is shown with a solid line, and the velocities of the positions with half the peak emission are shown with dashed lines. *c*: [S II] 6717/6731 line ratio as a function of distance from the source (integrated over all of the radial velocity range in which line emission is detected). *d*: The same as (c), but for the ([S II] 6717+31)/H α line ratio.

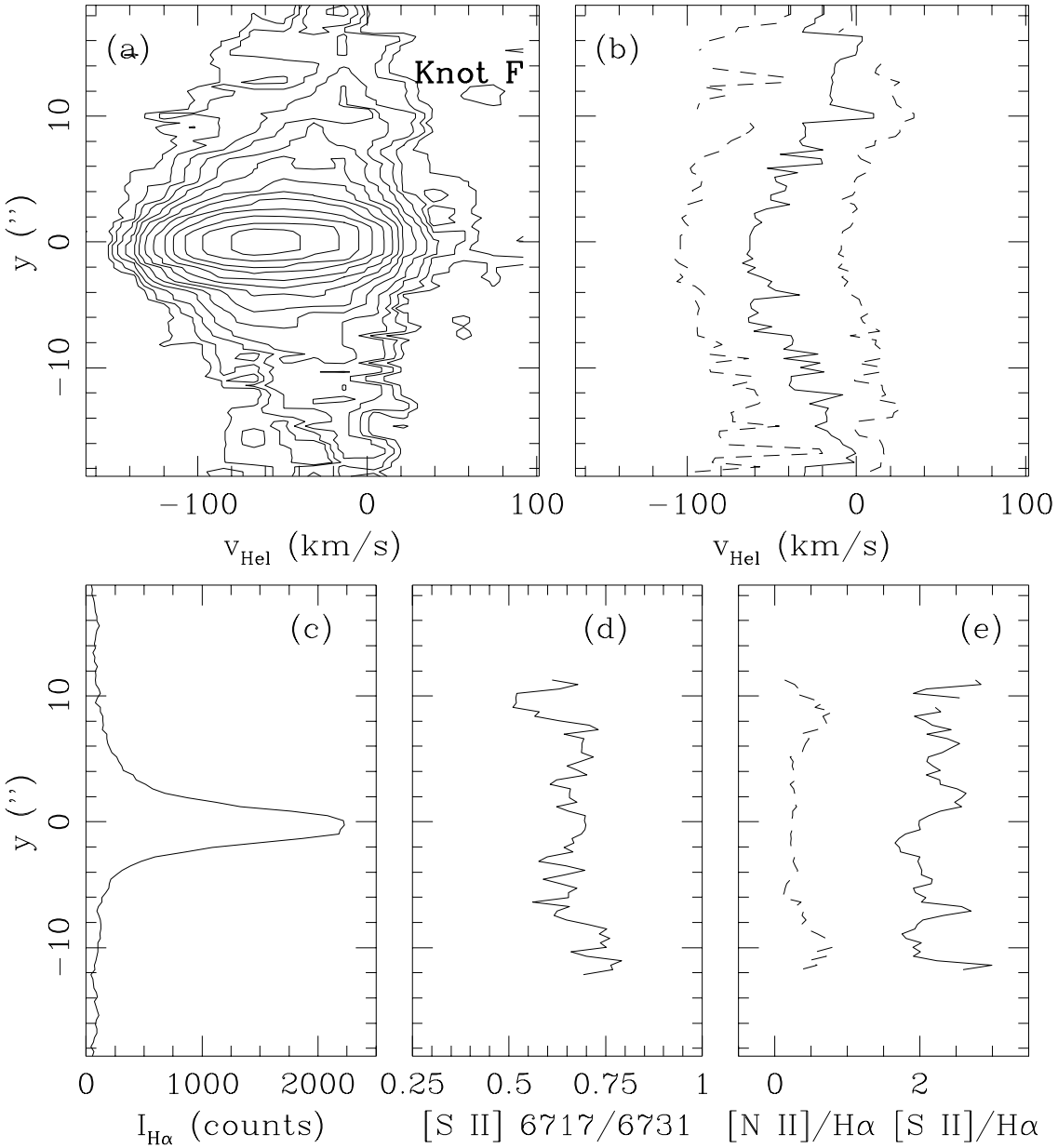


Fig. 3. *a*: [S II] 6731 long slit spectrum across the beam of the HH 111 jet at the position of knot F (slit position 2 of Figure 1), depicted with factor of $\sqrt{2}$, logarithmic contours. *b*: The heliocentric radial velocity corresponding to the peak of the line profile is shown with a solid line, and the velocities of the positions with half the peak emission are shown with dashed lines. *c*: H α intensity (integrated over all of the radial velocity range in which line emission is detected) as a function of distance from the central axis of the HH 111 jet. *d*: [S II] 6717/6731 line ratio through the cross section of the jet. *e*: The same as (c), but for the ([S II] 6717+31)/H α line ratio.

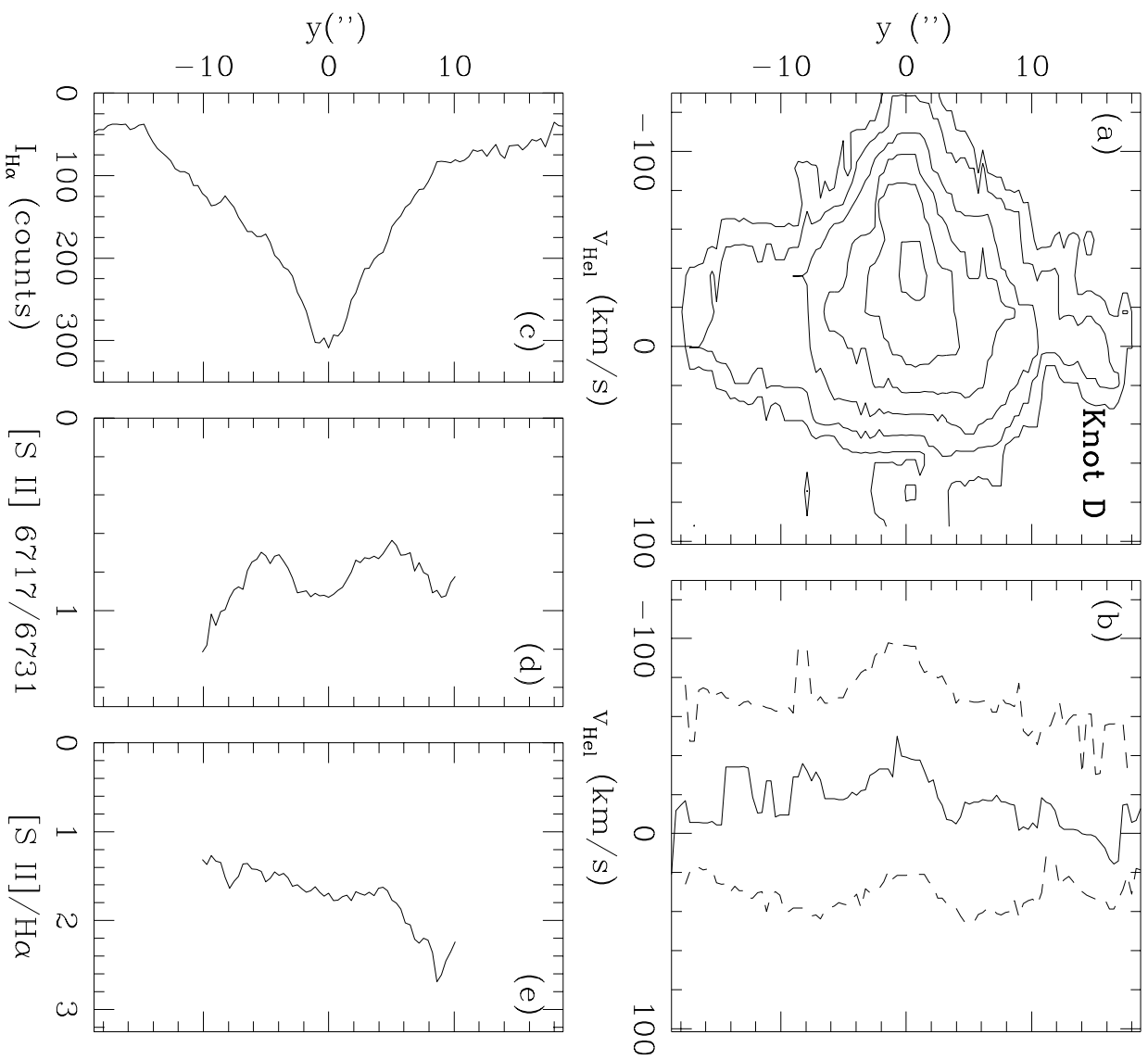


Fig. 4. The same as Figure 3, but for a cut across the HH 111 jet at the position of knot D (slit position 3 of Figure 1).

In the position-velocity diagrams, we see clear evidence of emission extending out to $\pm 16''$ from the center of the jet beam for knot F, and out to $\pm 14''$ for knot D. Through a comparison with the point spread function of a stellar source (which is also visible in the spectrum obtained through slit 1, see Fig. 1), we see that the emission is indeed extended, and not only a result of the rather low angular resolution of our observations (which had a seeing of $\approx 2\text{--}3''$, see § 2).

In knot F (Fig. 3a and b), we see a clear trend of decreasing radial velocities when moving away from the central axis of the HH 111 jet. In the central regions of the jet beam we measure a heliocentric velocity of the line peak of -60 km s^{-1} , and at $\approx \pm 12''$ from the jet axis this velocity has a value of -15 km s^{-1} . In all of the region with detected emission, the full line width at half maximum has an approximately constant value of $\approx 100 \text{ km s}^{-1}$. If we consider an inclination of the jet axis with respect to the plane of the sky of 10° (Reipurth et al. 1992) and a heliocentric velocity of $+8.5 \text{ km s}^{-1}$ for the ambient molecular cloud (Lee et al. 2000), we would conclude that the velocity of the jet relative to the ambient cloud drops from a central value of 395 km s^{-1} to a value of 135 km s^{-1} at a distance $\approx 5400 \text{ AU}$ away from the jet axis.

In knot D (Figure 4a and b), the on-axis heliocentric velocity of the line peak has a value of -40 km s^{-1} , and drops to a value of $\approx -20 \text{ km s}^{-1}$ at a distance of $\approx \pm 6''$ from the jet axis (while at such a distance from the axis, the velocity observed for knot F has a value almost equal to the axial velocity, see Fig. 3). Deprojecting these velocities, these values would correspond to a drop from a central velocity of 280 km s^{-1} relative to the ambient cloud to a velocity of 160 km s^{-1} at a distance of $\approx 2700 \text{ AU}$ from the jet axis. At larger distances, the signal-to-noise ratio of the line profile is very low, and the measured radial velocities are not reliable. The full width at half maximum of the line profile has an approximately position-independent value of $\approx 100 \text{ km s}^{-1}$.

Knot F (Fig. 3d) has an almost constant [S II] 6717/6731 ≈ 0.6 line ratio, corresponding to an electron density $n_e \approx 4500 \text{ cm}^{-3}$. Fig. 3e shows the [N II] 6583/H α and [S II] (6717+6731)/H α emission line ratios in knot F as a function of distance across the jet. The [N II] 6583/H α line ratio has a value of ≈ 0.2 for distances $< 7''$ from the jet axis, and has two symmetric peaks of ≈ 0.75 at distances of $8''\text{--}10''$ on both sides of the jet axis. The [S II] (6717+6731)/H α line ratio shows quite strong variability, ranging between values of 1.8 and

2.3. There appears to be a systematic trend in the [S II] (6717+6731)/H α line ratio, with higher values to the north of the HH 111 axis, and lower values to the south.

Such a north-south trend is clearly seen across knot D (Figure 4e), in which the [S II] (6717+6731)/H α ratio decreases from a value of ≈ 2.5 at a position of $10''$ to the north of the jet axis, to a value of ≈ 1.4 at $10''$ to the south of the jet axis. In this knot, we measure a ratio [S II] 6717/6731 ≈ 0.9 (corresponding to $n_e \approx 1000 \text{ cm}^{-3}$) within $\pm 2''$ from the axis, and lower values of ≈ 0.7 (corresponding to $n_e \approx 2500 \text{ cm}^{-3}$) at distances of $3''$ to $7''$ on both sides of the jet axis. At larger distances from the axis, the [S II] 6717/6731 ratio increases again to values of ≈ 1 at a distance of $\pm 10''$, indicating a drop of the electron density to $n_e \approx 700 \text{ cm}^{-3}$.

3.3. Excitation and Density Distribution as a Function of Velocity

The highest speeds are found along the axis of the jet (see § 3), and velocities about $20\text{--}40 \text{ km s}^{-1}$ smaller than the axial velocity are found along the edges of the emitting region. In the following, we study if this velocity structure is also accompanied by a change in the [S II] (6717+6731)/H α and [S II] 6717/6731 ratios. We have computed the [S II] (6717+6731)/H α and [S II] 6717/6731 ratios as a function of velocity for the central body of the jet (integrating the line intensities in a region covering $\pm 4''$ on each side of the jet axis), and for the edge of the jet (integrating the line intensities in a region from $4''$ to $10''$ to the north of the jet axis). In order to increase the signal-to-noise ratio, we have also binned the emission into five velocity channels with 40 km s^{-1} width. The line ratios obtained are shown as a function of heliocentric velocity in Figures 5 (knot F) and 6 (knot D).

In knot F, the [S II] (6717+6731)/H α ratio across the knot increases with increasing velocity relative to the ambient molecular cloud. As can be seen in Figure 5a, this ratio increases from 0.8, for heliocentric velocities around 20 km s^{-1} (low-velocity gas relative to the ambient molecular cloud, whose heliocentric velocity is $+8.5 \text{ km s}^{-1}$), to 3.6, for heliocentric velocities around -120 km s^{-1} (corresponding to high-velocity gas). Interestingly, Raymond et al. (1994) found a similar behaviour for the HH 46/47 jet, with a variation of the [S II] (6717+6731)/H α ratio by a factor of 4 across the jet.

In knot D, the [S II] (6717+6731)/H α ratio as a function of velocity is qualitatively similar in both the inner and outer regions (see Figure 6a). The

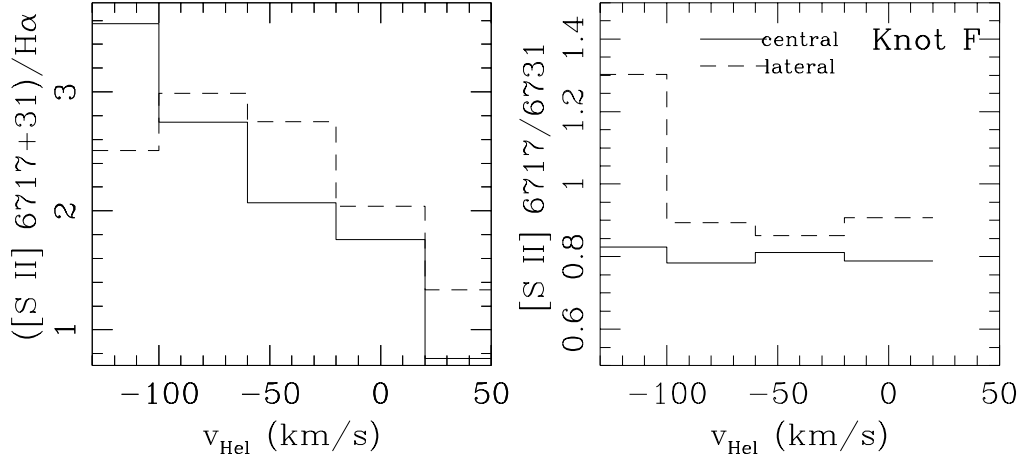


Fig. 5. [S II] (6717+6731)/H α (left) and [S II] 6717/6731 (right) line ratios as a function of radial velocity, calculated with the line intensities integrated over the central $y = -4 \rightarrow 4''$ region (solid lines) and lateral $y = 4 \rightarrow 10''$ region (dashed lines) of the cross section of the HH 111 jet at the position of knot F (slit position 2 of Figure 1).

gas approaching the observer at the highest velocity ($V_{\text{hel}} \approx -120 \text{ km s}^{-1}$) shows the highest [S II] (6717+6731)/H α ratios (from ≈ 2.1 to 2.8). The gas with heliocentric velocities from -80 to 0 km s^{-1} is characterized by an increase of the [S II] (6717+6731)/H α ratio with decreasing velocity relative to the ambient cloud.

We also find that the electron density in knot F, estimated from the [S II] 6717/6731 ratio, is almost velocity independent (with a value of 0.8, corresponding to $n_e \approx 1500 \text{ cm}^{-3}$) in the central region of the jet beam (see Figure 5b). In the outer region of this knot, [S II] 6717/6731 ≈ 0.7 (corresponding to $n_e \approx 2500 \text{ cm}^{-3}$) for velocities in the range -80 to 0 km s^{-1} , while at high velocities ($\approx -120 \text{ km s}^{-1}$) the ratio increases to ≈ 1.3 (corresponding to $n_e \approx 200 \text{ cm}^{-3}$).

In knot D, the trend of density as a function of velocity is similar in the inner region of the jet and in the edges of the jet (see Figure 6b). The electron density of the gas at velocities from -120 to 0 km s^{-1} increases with decreasing velocity relative to the ambient cloud. The highest electron densities are found for the material at heliocentric velocity of $\approx 0 \text{ km s}^{-1}$, and have $n_e \approx 1500 \text{ cm}^{-3}$, and the lowest electron densities are $n_e \approx 40$ and 700 cm^{-3} (for the edges and the center of the jet beam, respectively).

Interestingly, in both knots (F and D) we detect a faint, red wing in the emission line profile. This red wing is characterized by high [S II] 6717/6731 values (which approximately coincide with the low density limit) and low [S II] (6717+6731)/H α ratios. However, the line ratios measured in this faint, red

wing are quite uncertain.

4. DISCUSSION

In the previous section, we have presented the results that we have derived from long-slit spectra obtained with spectrograph slits 2 and 3 (see Fig. 1), which cut the HH 111 jet approximately at the positions of knots F and D, respectively. These spectra show a strong, central component (corresponding to the position where the slits cut the beam of the jet), and a faint, extended emission on both sides of the jet beam. There could be some question about the reality of this extended component. In particular, the HH 111 jet is embedded in a region with diffuse H α emission, and the extended component could in principle be part of this diffuse emission which has been left behind in the background subtraction procedure. However, the facts that the extended component is centered on the beam of the jet, and that it is kinematically related to the jet (see below) indicate that it is not merely an artifact of an incorrect background subtraction.

Let us summarize the results from the spectra obtained through slits 2 and 3 (see Fig. 1):

- We observe faint emission, extending for $\approx \pm 14''$ from the jet axis for knot D, and extending for $\approx \pm 16''$ for knot F. Knot F has a central, high intensity region, with a full width at half maximum of $\approx 3''$, which is unresolved with our angular resolution, and faint, extended wings at larger distances from the flow axis. Knot D shows a more gradual intensity versus position dependence.

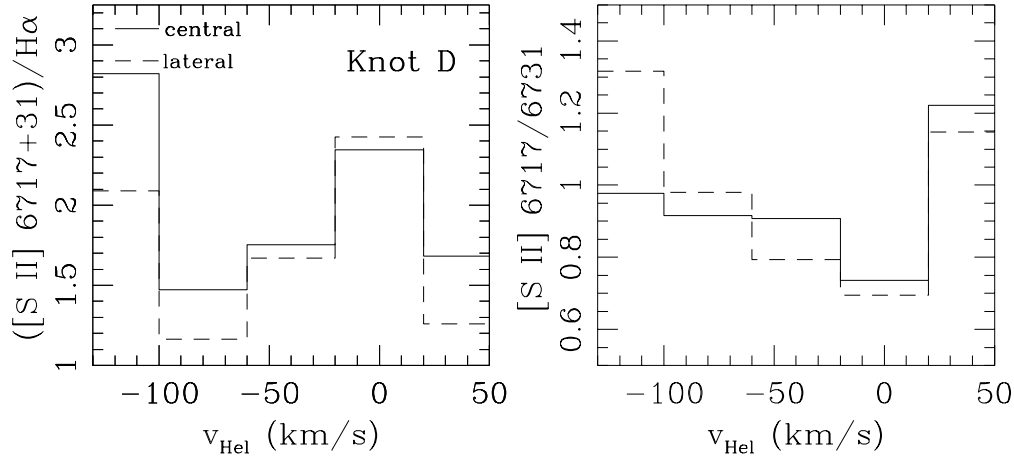


Fig. 6. The same as Figure 5, but for knot D (slit position 3 of Figure 1).

- We observe a radial velocity stratification, with higher velocities relative to the ambient cloud (heliocentric velocities of -60 and -40 km s^{-1} for knots F and D, corresponding to deprojected velocities relative to the ambient cloud of 395 and 280 km s^{-1} , respectively) on the jet axis, and lower velocities away from the axis.
- In knot D (at an angular distance of $\approx 22''$ or $10,000$ AU from the source) the radial velocity drops to a value of ≈ -20 km s^{-1} (corresponding to a deprojected velocity of 160 km s^{-1} relative to the ambient cloud) at a distance of $\approx 6''$ (2700 AU) from the jet axis. In knot F (at an angular distance of $\approx 27''$ or $12,000$ AU from the source) a radial velocity of ≈ -15 km s^{-1} is reached at $\approx 12''$ (5400 AU) from the jet axis.
- The full width at half maximum of the lines have an approximately position independent value of ≈ 100 km s^{-1} through both knots F and D.
- The [S II] (6717+6731)/H α ratio shows a decrease along the north-south direction in knot D, and a less clear, but similar effect across knot F.
- The [S II] 6717/6731 line ratio is surprisingly constant along the spectrograph slit cutting knot F (indicating an almost constant electron density $n_e \approx 4500$ cm^{-3}).
- This line ratio has a more complex behaviour across knot D, indicating the presence of an inner and outer region with $n_e \approx 1000$ cm^{-3} separated by a more dense, $n_e \approx 3000$ cm^{-3} “tube” extending from $3''$ to $7''$ from the jet axis.
- The line ratios as a function of radial velocities show a high velocity component with lower densities (from the [S II] 6717/6731 line ratio) and lower excitation (from the [S II] (6717+6731)/H α ratio) than the lower velocity gas.

Both the intensity and the transversal radial velocity profiles of knots D and F might be consistent with models in which a central, high velocity jet is surrounded by a slower velocity envelope. Such trends might arise from a situation in which a jet entrains surrounding, environmental material (see, e.g., Raga et al. 1993), or from a situation in which a jet with a strong transverse velocity structure is produced by the ejection mechanism (as in the “jet+disk wind scenario”, see, e.g., Kwan & Tademaru 1988; Lavalley et al. 1997). Interestingly, some of the MHD disk wind models do not appear to produce flows with a transversal increase of velocity toward the flow axis (Shu et al. 1995), while others do show this property (Ferreira 1997).

The more surprising result that we obtain is that the [S II] 6717/6731 line ratio indicates either a constant electron density across the jet cross section (as in knot F) or an increase of the electron density at distances of $3''$ - $7''$ from the jet axis (as in knot D), which points to the presence of an ionized envelope of high electron density around the jet. At the same time, the excitation of the spectrum does not change dramatically across the beam of the jet (with a [S II] (6717+6731)/H α ratio ranging from 2 to 2.5 in knot F and ranging from 1.4 to 2.5 in knot D, with a clear north-south asymmetry).

The lack of a strong change in the excitation of

the spectrum through the jet cross-section indicates that both the temperature and the ionization fraction are approximately independent of distance from the jet axis (of course, unless one has, e.g., temperature and ionization fraction changes which compensate each other in order to produce an invariant line ratio, which seems unlikely). Since the electron density, ionization fraction and temperature are approximately constant out to $\approx 10''$ away from the axis, one would naively expect that the line intensities should not decrease very rapidly away from the axis. This expectation is of course against what we observe in knot F, in which the line intensity cross sections are dominated by a strong, unresolved component centered on the jet axis (see Fig. 3c). This inconsistency appears to indicate that the filling factor of the emission has a strong decrease outwards from the jet axis. In this way, we would conclude that the strong decrease in intensity away from the jet axis in knot F approximately follows a corresponding decrease in the filling factor of the emitting gas.

The situation is even more dramatic for knot D, in which a higher electron density is measured in a ring surrounding the more strongly emitting, central region of the jet. Consequently, we would expect an increase of the intensities of the emission lines at this high-density ring. In this case, a strong decrease in the filling factor of the emitting material within this ring would be necessary to explain the low line emission in the regions at distances $> 3''$ from the jet axis.

5. CONCLUSIONS

In deep, long-slit spectra obtained across the outflow axis of the HH 111 jet, we have detected line intensity and radial velocity gradients extending out to $\approx \pm 15''$ from the flow axis. This region coincides spatially with the CO-emitting “tube” which surrounds the beam of the HH 111 optical jet (Cernicharo & Reipurth 1996; Cernicharo, Neri, & Reipurth 1997; Nagar et al. 1997). We find that this extended emission has peculiar properties, with a strongly decreasing intensity out from the jet axis, but with an approximately constant excitation and electron density. These apparently contradictory properties indicate that there is probably a strong decrease in the filling factor of the emitting gas as a function of increasing distances from the jet axis.

At the same time, we detect a strong decrease in velocity, ranging from a central velocity of 280 km s^{-1} to an edge velocity of 160 km s^{-1} for knot D, and from 395 km s^{-1} to an edge velocity of 135 km s^{-1} for knot F (these velocities correspond to deprojected velocities relative to the ambient cloud). The veloc-

ity decrease occurs over a half-width of $\approx 2700 \text{ AU}$ for knot D (located at $\approx 10,000 \text{ AU}$ from the source) and over a half-width of $\approx 5400 \text{ AU}$ for knot F (located at $\approx 12,000 \text{ AU}$ from the source). This result appears to indicate that the low velocity, outer envelope of the jet has a dramatic sideways expansion between knot D (located in the region in which the jet emerges from the high extinction core surrounding the central source, see Reipurth et al. 1992) and knot F. In this region, the central part of the jet also shows a dramatic velocity increase (from 280 km s^{-1} in knot D to 390 km s^{-1} in knot F, also see Reipurth et al. 1997).

Extended, low velocity emission surrounding the jet beam has also been detected along the full length of the HH 46/47 jet (Hartigan et al. 1993) and within $\approx 6''$ from the source of the DG Tau jet (Mundt et al. 1987; Lavalley et al. 1997). The position-velocity diagrams obtained for these flows across the jet are qualitatively quite similar to the ones that we have obtained for HH 111.

It is in principle possible to interpret these observational results in terms of either a jet beam with an increase in the outflow velocity in the transverse direction toward the flow axis, or a central jet entraining low velocity, environmental material. It will be necessary to attempt to carry out appropriate predictions from gas-dynamic models of these types of flow to see whether or not results consistent with the present observations are obtained.

A third possibility is that the extended emission that we are observing around the jet beam (extending out to $\pm 12''$ from the jet axis) corresponds to dispersion by dust present in the CO emitting “tube” around the HH 111 jet (Cernicharo et al. 1997; Nagar et al. 1997). If the light that is being dispersed is the emission from the jet, we would expect a strong increase of the velocity dispersion as we move away from the jet axis (see Calvet et al. 1992; Henney, Raga, & Axon 1994), and such an effect is not seen in our position-velocity diagrams (see Figs. 3 and 4). The other possibility is that we are observing the dispersion of light emitted by the regions of the outflow close to the source, in which case the limited range of possible lines of sight would produce a small velocity dispersion. However, the fact that the region surrounding the HH 111 jet beam does not show evidence for high electron densities and low ($[\text{S II}] 6717+6731/\text{H}\alpha$) line ratios (as would be expected for the region close to the outflow source, see, e.g., the observations of Lavalley et al. 1997) appears to be a problem for this interpretation.

The conclusion therefore appears to be that there

is a quite broad region around the beam of the jet which partially shares the kinematical properties of the jet (having radial velocities ranging from the jet velocity down to low velocities at distances greater than $10''$ from the jet axis). If correct, this result is most interesting, as it challenges most of the current models, in which the jet has a well defined, narrow beam. However, we think that the results should be taken with some caution, as the current observations have a rather low angular resolution, and that they should be verified with future observations.

We thank Alberto Noriega-Crespo who provided us with the F673N HST image of HH 111. This work was funded through grant ACI 2000-8 from the Direcció General de Recerca, PB98-0670 grant from the Spanish DGICYT, and TIC 126 grant from Junta de Andalucía. The work of ACR was supported by the CONACyT grant 32753-E, and by a fellowship of the John Simon Guggenheim Memorial Foundation. Finally, we thank Bo Reipurth (the referee) for helpful comments.

REFERENCES

- Aller L. H. 1984, *Physics of Thermal Gaseous Nebulae* (Dordrecht: Reidel)
- Bacciotti, F., Mundt, R., Ray, T. P., Eisloffel, J., Solf, J., & Camenzind, M. 2000, *ApJ*, 537, L49
- Calvet, N., Cantó, J., Binette, L., & Raga, A. C. 1992, *RevMexAA*, 24, 81
- Carter, D., et al. 1994, *WHT ISIS User's Manual*, Isaac Newton Group Telescopes, Royal Greenwich Observatory
- Cernicharo, J., Neri, R., & Reipurth, B. 1997, in *IAU Symp. 182, Herbig-Haro Flows and the Birth of Low Mass Stars*, eds. B. Reipurth & C. Bertout (Boston: Kluwer), 141
- Cernicharo, J., & Reipurth, B. 1996, *ApJ*, 460, L57
- Eisloffel, J., & Mundt, R. 1992, *A&A*, 263, 292
- _____. 1994, *A&A*, 284, 530
- Ferreira, J. 1997, *A&A*, 319, 340
- Gredel, R., & Reipurth, B. 1994, *A&A*, 289, L19
- Hartigan, P., Morse, J. A., Heathcote, S., & Cecil, G. 1993, *ApJ*, 414, L121
- Heathcote, S., & Reipurth, B. 1992, *AJ*, 104, 2193
- Henney, W. J., Raga, A. C., & Axon, D. J. 1994, *ApJ*, 427, 305
- Kwan, J., & Tadamaru, E. 1988, *ApJ*, 332, L41
- Lavalley, C., Cabrit, S., & Dougados, C. 1997, *A&A*, 327, 671
- Lavalley-Fouquet, C., Cabrit, S., & Dougados, C. 2000, *A&A*, 356, L41
- Lee, C. F., Mundy, L. G., Reipurth, B., Ostriker, E. G., & Stone, J. M. 2000, *ApJ*, 542, 925
- Meaburn, J., & Dyson, J. E. 1987, *MNRAS*, 225, 863
- Morse, J. A., Heathcote, S., Hartigan, P., & Cecil, G. 1993, *AJ*, 106, 1139
- Mundt, R., Brugel, E. W., & Bührke, T. 1987, *ApJ*, 319, 275
- Nagar, N. M., Vogel, S. N., Stone, J. M., & Ostriker, E. C. 1997, *ApJ*, 482, L195
- Raga, A. C., Cantó, J., Calvet, N., Rodríguez, L. F., & Torrelles, J. M. 1993, *A&A*, 276, 539
- Raymond, J. C., Morse, J. A., Hartigan, P., Curiel, S., & Heathcote, S. 1994, *ApJ*, 434, 232
- Reipurth, B. 1989, *Nature*, 340, 42
- Reipurth, B., Hartigan, P., Heathcote, S., Morse, J. A., Bally, J. 1997, *AJ*, 114, 757.
- Reipurth, B., Raga, A. C., & Heathcote, S. 1992, *ApJ*, 392, 145
- Rodríguez, L. F., & Reipurth, B. 1994, *A&A*, 281, 882
- Shu, F. H., Najita, J., Ostriker, E. C., & Shang, H. 1995, *ApJ*, 455, L155
- G. Anglada: Instituto de Astrofísica de Andalucía, CSIC, Apdo. de Correos 3004, E-18080 Granada, Spain (guillem@iaa.es).
- R. Estalella and R. López: Departament d'Astronomia i Meteorologia, Universitat de Barcelona, Av. Diagonal 647, E-08028 Barcelona, Spain (robert.rosario@am.ub.es).
- A. C. Raga: Instituto de Astronomía, Universidad Nacional Autónoma de México, Apartado Postal 70-264, 04510 México, D. F., México (raga@astroscu.unam.mx).
- A. Riera: Departament de Física i Enginyeria Nuclear, Universitat Politècnica de Catalunya, Av. Víctor Balaguer s/n, E-08800 Vilanova i la Geltrú, Spain (angels.riera@upc.es).